Loss of *Drosophila melanogaster p21-activated kinase 3* Suppresses Defects in Synapse Structure and Function Caused by *spastin* Mutations

Emily F. Ozdowski,* Sophia Gayle,* Hong Bao,† Bing Zhang,† and Nina T. Sherwood*,[1]
*Department of Biology/Institute for Genome Sciences and Policy, Duke University, Durham, North Carolina 27710 and
†Department of Zoology, University of Oklahoma, Norman, Oklahoma 73019

ABSTRACT Microtubules are dynamic structures that must elongate, disassemble, and be cleaved into smaller pieces for proper neuronal development and function. The AAA ATPase Spastin severs microtubules along their lengths and is thought to regulate the balance between long, stable filaments and shorter fragments that seed extension or are transported. In both *Drosophila* and humans, loss of Spastin function results in reduction of synaptic connections and disabling motor defects. To gain insight into how *spastin* is regulated, we screened the *Drosophila melanogaster* genome for deletions that modify a *spastin* overexpression phenotype, eye size reduction. One suppressor region deleted *p21-activated kinase 3* (*pak3*), which encodes a member of the Pak family of actin-regulatory enzymes, but whose *in vivo* function is unknown. We show that *pak3* mutants have only mild synaptic defects at the larval neuromuscular junction, but exhibit a potent genetic interaction with *spastin* mutations. Aberrant bouton morphology, microtubule distribution, and synaptic transmission caused by *spastin* loss of function are all restored to wild type when *pak3* is simultaneously reduced. Neuronal overexpression of *pak3* induces actin-rich thin projections, suggesting that it functions *in vivo* to promote filopodia during presynaptic terminal arborization. *pak3* therefore regulates synapse development *in vivo*, and when mutated, suppresses the synaptic defects that result from *spastin* loss.

REGULATION of the neuronal microtubule cytoskeleton is critical for proper process outgrowth, intracellular transport, and synapse modification. Microtubule misregulation is observed in many human neurodegenerative disorders, including Alzheimer's disease and amyotrophic lateral sclerosis (Warita *et al.* 1999; Reid *et al.* 2002; Stamer *et al.* 2002). Many aspects of microtubule dynamics are well understood, such as growth by polymerization of tubulin subunits and destruction by catastrophe of microtubule filaments (reviewed in Wade 2009). However, much remains to be elucidated about an additional mechanism of regulation, microtubule severing, and the motoneuron disease that results from its loss.

Autosomal dominant hereditary spastic paraplegia (AD-HSP) is a progressive neurodegenerative disease that primarily affects the distal ends of the longest motor axons of the central nervous system (CNS) (Fink *et al.* 1996). This localized degeneration results in debilitating leg weakness and progressive loss of patient mobility. While multiple genes contribute to this phenotype, the majority of AD-HSP mutations are located in *spastin*, which encodes an AAA ATPase that binds and severs microtubules (Hazan *et al.* 1999; Errico *et al.* 2002). Although the disorder is dominantly inherited, onset age and severity vary widely. Even within a single pedigree, the onset of mobility problems can range from early childhood to late in adulthood, suggesting that additional genetic or epigenetic factors play key roles in the phenotypic severity of the disease. Environmental correlations have not been reported. However, evidence for additional genetic contributions is seen in several independent pedigrees, where single nucleotide polymorphisms encoding missense changes S44L or P45Q in the Spastin protein itself dramatically enhance disease severity when they occur in *trans* with a mutation affecting Spastin's catalytic domain (Chinnery *et al.* 2004; Svenson *et al.* 2004; Naimi *et al.* 2005; McDermott *et al.* 2006; Schickel *et al.* 2007).

doi: 10.1534/genetics.111.130831
Manuscript received May 18, 2011; accepted for publication June 13, 2011
Supporting information is available online at http://www.genetics.org/content/suppl/2011/06/24/genetics.111.130831.DC1.
[1]Corresponding author: Duke University Medical Center, CARL Bldg., Box 3577, Durham, NC 27710. E-mail: ntangs@duke.edu

To elucidate the details of Spastin function in the nervous system, we employ the model organism *Drosophila melanogaster*. The fruit fly has proven an excellent model for studying the roles and regulation of *spastin* (*spas*); not only is there high amino acid sequence similarity between human and *Drosophila* Spastin (67% identity within the critical ATPase domain; Kammermeier *et al.* 2003), but the fly *spastin* null phenotype of leg weakness and failure to jump or climb bears striking similarity to the characteristic mobility symptoms of AD-HSP patients. As in vertebrates, *Drosophila* Spastin protein severs microtubules (Roll-Mecak and Vale 2005). *spastin* null larvae exhibit weakened synaptic transmission at the neuromuscular junction (NMJ), as well as irregular clusters of synaptic boutons at the distal tips of axons, which contain insufficient microtubule arrays (Sherwood *et al.* 2004). Moreover, expression of wild-type human Spastin rescues these larval defects, while expression of human disease mutations recapitulates the allelic progression of severity in AD-HSP (Du *et al.* 2010). Thus, discoveries of *spastin* function and regulation in the fly are likely to reveal important mechanistic insights into its role in humans.

Previous studies addressing Spastin regulation have used biochemical approaches to identify protein interactions between Spastin and members of the endosomal sorting and membrane trafficking machinery, centrosomal components, as well as other proteins implicated in AD-HSP (Errico *et al.* 2004; Reid *et al.* 2005; Evans *et al.* 2006; Mannan *et al.* 2006a,b; Sanderson *et al.* 2006). Genetic screens for key components that interact with *spastin* in the intact nervous system, however, have not been pursued and represent an important complementary approach toward understanding *spastin* function *in vivo*.

The p21-activated kinases (Paks), a family of serine/threonine kinases that serve as Rac/Cdc42 effectors, regulate the actin cytoskeleton in many developmental processes and are evolutionarily conserved from yeast to humans. The *Drosophila* genome encodes three Pak proteins: two of these, *dPak* and *mushroom bodies tiny* (*mbt*), fit strongly into conserved structural subtypes (types 1 and 2, respectively; Jaffer and Chernoff 2002; Bokoch 2003), while the last, *p21-activated kinase 3* (*pak3*), is loosely related to type 1 ("type 1*"; Mentzel and Raabe 2005). Roles for *dPak* have been demonstrated in axon guidance of photoreceptor and olfactory neurons (Hing *et al.* 1999; Newsome *et al.* 2000; Ang *et al.* 2003) and in coordinating the maturation of postsynaptic terminals at the *Drosophila* NMJ (Albin and Davis 2004). Additionally, *dPak*'s roles extend beyond the nervous system, to dorsal closure, myotube guidance, and F-actin polarization in ovarian follicle cells (Conder *et al.* 2004, 2007; Bahri *et al.* 2009). *mbt* is similarly implicated in nervous system development, including neurogenesis and photoreceptor morphogenesis, but in roles distinct from *dPak* (Melzig *et al.* 1998; Schneeberger and Raabe 2003; Menzel *et al.* 2007). In contrast to these diverse functions of *dPak* and *mbt*, *pak3* remains uncharacterized *in vivo*. In cultured *Drosophila* S2 cells, *pak3* overexpression induces extensive filopodial formation, while reduction results in a polarized lamellipodial distribution of actin filaments and induction of migration (Asano *et al.* 2009).

We screened the *Drosophila* genome for interactions with *spastin* overexpression, and identified *pak3* as a genetic regulator of *spastin* function *in vivo*. Ectopic *spastin* expression in the eye resulted in surface area reduction and defective morphology. Progeny of these flies, crossed to those bearing genomic deletions, revealed regions that enhanced or, in the case of *pak3*, suppressed the abnormal eye phenotype caused by *spastin* overexpression. To understand *pak3* function *in vivo*, we analyzed the effects of both its genetic loss of function and neuronal overexpression at the larval NMJ as well as its loss of function in conjunction with *spastin* mutations. While *pak3* mutations alone only mildly affected the NMJ, loss of *pak3* completely suppressed *spastin* mutant phenotypes, including microtubule distribution, synapse morphology, and synaptic function.

Materials and Methods

Drosophila stocks and sources

Spastin overexpression in the eye was achieved using *glass multimer reporter (GMR)*-GAL4 to drive *P{EP}spastin^{T32}* (Sherwood *et al.* 2004). Two transposable element insertion lines, *P{XP}pak3^{d02472}* and *PBac{RB}pak3^{e00329}*, were obtained from the Harvard collection of Exelixis stocks. Although the original *pak3^{d02472}* line was homozygous lethal, backcrossing to *w^{1118}* for five generations removed the lethality, presumably by recombining away a second site mutation. *pak3^{e00329}* was also backcrossed to obtain a comparable genetic background. The *pak3* RNAi line, *P{GD8481}v39844*, was acquired from the Vienna *Drosophila* RNAi Center. The UAS insertion, *P{Mae-UAS.6.11}pak3^{LA00012}*, as well as aberration lines *Df(3R)Exel6269* and *Exel9055*, were from the Bloomington Drosophila Stock Center. The control lines used were *w*; Canton S (WCS) for morphology and *w^{1118}* for electrophysiology. All lines were kept on yeast-sugar-agar media at room temperature (~22°). *Df(3R)pak3* was produced according to Parks *et al.* 2004, using *P{hsFLP}1*, *y^{1} w^{1118}*; *Dr^{1}/TM3*, *Sb^{1}* (BL 26902), *w*; *P{XP}pak3^{d02472} / TM6b* (after backcrossing), *w*; *PBac{RB}pak3^{e00329}/TM6b* (after backcrossing), and *w^{1118}*; *P{hs-hid}3*, *Dr^{1}/TM6B*, *Tb^{1}* (BL7758). Heat shock was performed on first, second, and third instar larvae for 2 hr on 4 consecutive days. Adults were examined for loss of {*w^{+}*} eye color, a balanced stock was established, and genomic DNA was amplified by PCR to confirm the presence of a hybrid transposable element and the loss of *pak3* (as described below).

Genetic combinations were achieved by recombining *pak3* mutations with the *spastin$^{5.75}$* deletion (*Df(3R)pak3*, *spas$^{5.75}$* line 54; *pak3^{d02472}* (original), *spas$^{5.75}$* line 15; *pak3 ^{d02472}* (backcrossed), *spas$^{5.75}$* line 17). For both immunocytochemical and electrophysiological assays, parents carrying the appropriate *pak3* and *spastin* alleles balanced by *TM6b*

Tb[1] *Antp*[Hu] were crossed and wandering third instar larvae lacking the *Tb* marker selected.

Analyses of neurons overexpressing *pak3* were performed by dissecting GFP-negative wandering third instar progeny of *elav-Gal4/CyO twist-Gal4*, *UAS-GFP* flies crossed to *P{Mae-UAS.6.11}pak3*[LA00012] homozygotes. Actin filaments were observed using additional transgenes, *UAS-GMA* (GFP:Moesin actin-binding domain, kind gift of D. Kiehart, Duke University, Durham, NC) and *UAS-Act5c:GFP* (BL7310).

PCR

Hybrid transposable elements, the result of FRT-induced deletions between P{XP} and PBac{RB} insertions, are recognized by the primer AATGATTCGCAGTGGAAGGCT (XP specific, as published in Parks *et al.* 2004), in conjunction with CCAATGCGTTTATTTCAGGTCACG (RB specific, as recommended by K. Cook of the Bloomington Drosophila Stock Center). Further primer combinations also confirmed *pak3* deletion: CGCGAATTAACCTTTAGGC in the *pak3* 5′-UTR with the XP-specific primer, and the RB-specific primer with either flanking genomic primer, AGCTGTACTTTGCCC CAAGA or TACTCACACACGCAGGGAAA, both located in the intron. These primer combinations showed that *Exel9055* lacks a hybrid element and does not delete *pak3*, and that *Df(3R)pak3* contains a hybrid element and deletes *pak3*.

Deficiency screen

GMR-Gal4/GMR-Gal4 ; *spas*[T32]*/TM6b* flies were crossed to individual deletions of chromosomes X, 2, 3, and 4 of the Bloomington deficiency kits available in 2004. Progeny heterozygous for the deletion, *GMR-Gal4* and *spas*[T32] were compared to their sibling controls heterozygous for *GMR-Gal4* and *spas*[T32] alone. Eye size, texture, and pigmentation were evaluated to determine the severity and direction of any genetic interaction: eyes with smaller size, smoother texture (indicating loss of ommatidia), or loss of pigmentation were considered more defective. Further screening was performed with Exelixis deficiencies and mutant alleles of candidate genes to narrow regions of interest. For potential interactors, heads were imaged at ×500 with a Fujifilm E550 camera at 4× optical zoom, and eye area was measured in ImageJ for quantification of eye reduction. Three traces for each eye image were averaged to minimize tracing error. All eye measurements of a given genotype were averaged and compared to other genotypes using a Student's *t* test for statistical significance.

Reverse transcription-PCR

A total of 30 third instar larvae of each genotype were flash frozen in liquid N_2, and RNA was isolated using the RNAspin Mini/Nucleospin kit (GE Healthcare/Clontech). RNA concentration was measured using UV spectrophotometry and 1 μg RNA was used for cDNA synthesis with Bioline reverse transcriptase. PCR amplification of *pak3* was performed with the following forward primers AAATGGCGAAAGCAGGACTA (Pak3 RTF) and CGCGAATTAACCTTTAGGC (Pak3 F) with the reverse primer GTGTTTGTGTGCGTTGTTGA (Pak3 R). Both primer pairs flank introns so that cDNA products are easily distinguishable from genomic DNA contamination. *pak3-C* unique transcripts were identified using Pak3 RTF with multiple downstream primers, including Pak3 R7, TGTCGGGTATGTTTCGGTTT.

PCR amplification of the loading control, *GAPDH2*, was performed with the following primers: GCAAGCAAGCCGA TAGATAAAC (GAPDH2 RTF) and TCGATGAAGGGATCGTT GAC (GAPDH2 RTR). GAPDH2 RTF primer sequence spans the exon–intron border so that only cDNA is amplified.

Eclosion rate

Balanced *pak3* alleles were crossed in every combination and adult progeny quantified. The percentage of total progeny for a given genotype was compared to the percentage expected on the basis of the genetic cross. For example, in the cross *pak3*[d02472]*/TM6b* X *pak3*[e00329]*/TM6b*, 33% each of *pak3*[d02472]*/pak3*[e00329], *pak3*[d02472]*/TM6b*, and *pak3*[e00329]*/TM6b* were expected. Therefore, if 26% of the total progeny were *pak3*[d02472]*/pak3*[e00329], it is graphed as 79% of expected. Statistical significance was determined by χ^2 analysis.

Immunostaining

Wandering third instar larvae were filleted in phosphate-buffered saline (PBS, Invitrogen) and fixed in either Bouin's medium (5–10 min, Sigma) or 4% paraformaldehyde (45 min, EMD Chemicals). Fillets were washed in PBS with 0.2% Triton X-100 (PBST) and blocked in PBST with 5% normal goat serum, 0.01% bovine serum albumin, and 0.02% sodium azide for 1 hr at room temperature. Primary antibody was diluted in blocking solution and used at 4° overnight; secondary antibody incubation was for 2 hr at room temperature in the dark. Unless otherwise noted, primary antibodies used after paraformaldehyde fixation were monoclonals from the Developmental Studies Hybridoma Bank (DSHB), maintained by the University of Iowa, Department of Biological Sciences: anti-Futsch 22C10 (1:50; Bouin's), anti-glutamate receptor II (GluR IIA) 8B4D2 (1:100; Bouin's), anti-synapsin (Syn) 3C11 (1:100), anti-Discs-large (Dlg) 4F3 (1:100), anti-Brüchpilot (Brp) NC82 (1:50, 10-min fixation), and anti-GFP (1:300, Invitrogen). Rabbit anti-horseradish peroxidase (HRP; 1:100, Cappel) was used with either fixation. Secondary antibodies, goat anti-mouse Alexa 568, goat anti-mouse Alexa 488, goat anti-rabbit Alex 568, and goat anti-rabbit Alexa 488 (Molecular Probes) were used at 1:300.

Quantification of NMJ morphology

Total bouton number included all Ib and Is boutons at muscle 4 of each hemisegment, regardless of bouton size, branch length, or cluster structure. Terminal boutons were those at the distal tip of each branch, whether arranged linearly or within a cluster. A branch could include a single bouton as long as anti-HRP displayed membranous material

connecting it to the axon. The thin protrusions induced by Pak3 overexpression were included in the quantification of terminal boutons, although further anti-Dlg and anti-GluRIIA staining determined that they were not fully formed synapses. We defined a "bunch" as a cluster of similarly sized boutons that appeared like a bunch of grapes. These clusters were only found at the distal tips of axonal branches. The number of terminal boutons within a bunch was variable. Other cluster structures were possible, such as "starbursts" of small satellite boutons, but those were also found in wild type and are not quantified here.

Electrophysiology

The standard third instar larval body-wall muscle preparation first developed by Jan and Jan (1976) was used for electrophysiological recordings (Zhang *et al.* 1998; Bao *et al.* 2005). Wandering third instar larvae were submerged in ice-cold HL-3 saline (0.8 mM calcium; Stewart *et al.* 1994), incised with a sharp razor blade along the dorsal midline and held open on a magnetic dish with metal pins. After removal of internal organs and fat tissues, the remaining body-wall muscle and central nervous system was rinsed three times with fresh, cold HL-3 saline and bathed in room temperature HL-3. The nerve roots were cut near the exit site at the ventral nerve cord so that the motor nerve could be picked up by a suction electrode. The input resistance of the recording microelectrode (backfilled with 3 M KCl) ranged from 20 to 25 MΩ. Muscle synaptic potentials were recorded using an Axon Clamp 2B amplifier (Axon Instruments) and acquired by a Dell PC computer equipped with pClamp software. Following motor nerve stimulation with a suction electrode (100 μsec, 5 V), evoked excitatory junction potentials (EJPs) were recorded. Three to five EJPs evoked by low-frequency stimulation (0.1 Hz) were averaged. For mini recordings, TTX (1 μm) was added to prevent unwanted evoked release (Zhang *et al.* 1998). The Mini Analysis program (Synaptosoft) was used to measure the amplitude of individual miniature EJPs (mEJPs or minis). A total of 50–100 events per muscle were analyzed to obtain the average mEJP amplitude. Minis with a slow rise and falling time arising from neighboring electrically coupled muscle cells were excluded from analysis (Gho 1994; Zhang *et al.* 1998). Quantal content was determined by dividing the average EJP amplitude by mEJP amplitude for each muscle. Only muscles with a recorded input resistance ≥5 MΩ were analyzed. Data are presented as mean ± SEM and considered significantly different when $P < 0.05$ in unpaired Student's *t* tests.

Results

A genome-wide deficiency screen for dominant modifiers of spastin overexpression in the eye

Many successful genetic modifier screens have been conducted in *Drosophila* utilizing overexpression phenotypes in the eye (reviewed in Thomas and Wassarman 1999). We thus overexpressed endogenous *spastin*, under the control of the eye-specific driver, *GMR-Gal4*. Notably, *spastin* overexpression resulted in eye size reduction and smoother texture, presumably due to loss of the normal ommatidial lattice (Figure 1, A and B). We took advantage of this phenotype to identify potential mechanisms of *spastin* regulation by screening genomic deletion lines for genetic modifiers of the eye size reduction. The intermediate severity of the *spastin* eye phenotype allowed identification of both enhancing (Figure 1C) and suppressing (Figure 1D) interactions.

Genomic deletion lines across all chromosomes were screened using the Bloomington kit of cytologically defined deletions, which covered ~85% of the genome. Most interacting deletions changed the size, texture, or pigmentation of the reduced eye (Figure 1, C and D). We also identified one enhancer that resulted in ectopic, potentially necrotic, tissue consistently positioned in the anterior of the eye (Figure 1E). In total, we identified 6 enhancer and 10 suppressor regions. We have first focused on characterizing the suppressors, reasoning that rescue of the eye phenotype is likely to be highly specific to *spastin* function.

pak3 genetically interacts with spastin in the eye

To search for genes responsible for suppression of the *spastin* overexpression phenotype, overlapping deficiencies and individual mutant alleles were examined in the *spastin* overexpression background. With this strategy, we identified the suppressor at 89B-C as *p21-activated kinase 3* (*pak3*). Eye size for each *pak3* mutant allele combined with *spastin* overexpression was measured and compared to its *spastin*-overexpressing siblings (Figure 2A). The region deleted by the original suppressor, *Df(3R)Exel6269* (Figure 2B), comprised ~40 candidate genes. Tests of multiple lines within this region revealed that alleles of *pak3*, namely the deletion we constructed, *Df(3R)pak3* (Figure 2C), two insertion lines (Figure 2, D and E; Dietzl *et al.* 2007), and a UAS-dsRNA line (Figure 2F; Thibault *et al.* 2004), all suppressed the eye phenotype caused by *spastin* overexpression. Conversely, simultaneous overexpression of both *spastin* and *pak3* resulted in enhancement of the size reduction (Figure 2G). Quantification of these results (Figure 2H) showed that all changes were statistically significant (Student's *t* test, $P < 0.02$). We conclude that *pak3* interacts genetically with *spastin* in the eye.

Characterization of pak3 gene annotation and mutant alleles

D. melanogaster gene annotation predicts two transcriptional isoforms of *pak3* (Tweedie *et al.* 2009). *pak3-A*, a 3.2-kb transcript derived from two exons (Figure 3A), amplified robustly from whole embryos, larvae, and adults and was found in all tissues and developmental stages tested. *pak3-C*, a 5-kb transcript, differs from *pak3-A* only in the length of the 3′-UTR. It is expressed in embryonic, larval, and adult stages. The predicted protein-coding region for each transcript yields

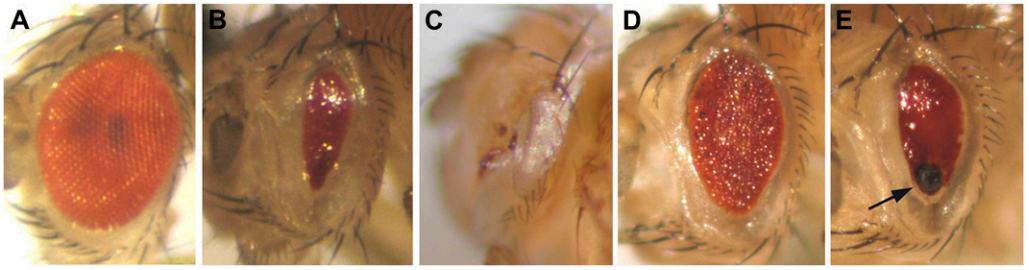

Figure 1 A deficiency screen for modifiers of the *spastin* overexpression eye phenotype. (A) Wild-type eye morphology is a bulbous structure made up of a regular array of ommatidia. (B) *GMR-Gal4/+*; *P{EP}spas*^{T32}/+ resulted in eye-specific overexpression of the *spastin* gene, which caused eye size reduction (both in area and depth) and loss of the ommatidial texture. Screening genomic deficiencies for modification of this *spastin*-induced intermediate phenotype uncovered enhancers of eye reduction, such as (C) *Df(3R)e-N19*, suppressors of eye reduction, such as (D) *Df(3R)Exel6269*, and new phenotypes, such as (E) the anterior necrosis (arrow) in *Df(1)Exel6227*. In each panel, anterior is to the left and all photos were taken at the same magnification.

the same polypeptide. Consistent with this result, Western blots probed with an anti-Pak3 antiserum reveal a single band in both males and females (Mentzel *et al.* 2009).

To determine the molecular nature of the *pak3* alleles, we examined genomic DNA from lines with P{XP} or PBac {RB} transposable element insertions or hybrid insertion elements after gene deletion. The genomic locations of the insertions, *pak3*^{d02472} and *pak3*^{e00329}, were in agreement with those reported (Figure 3A). However, the reported deletion, *Df(3R)Exel9055*, constructed by FLP-mediated recombination between the two inserts, was inconsistent with our PCR-amplification experiments. We tested for the hybrid insertion element that should have been produced by the Exelixis deletion (Parks *et al.* 2004); neither primers used in the original Exelixis screen nor new flanking primer pairs (see *Materials and Methods*) produced the appropriate product. This eliminated the possibility that *pak3* is deleted in *Df(3R)Exel9055*.

The severity of the remaining alleles was determined through semiquantitative measurement of larval mRNA expression by reverse transcription-PCR (RT-PCR). These tests revealed that *pak3* transcript was almost completely eliminated in *pak3*^{d02472} homozygotes and significantly reduced in *pak3*^{e00329} homozygotes (Figure 3B). Transcript was detected in *pak3*^{d02472} only after additional amplification cycles (data not shown). Finally, the *P{Mae-UAS.6.11}* insertion in *pak3*^{LA00012} did not disrupt *pak3* transcription, even though its insertion site within the 5′-UTR is close to that of *pak3*^{e00329}. On the basis of these data, *pak3*^{d02472} is a strong hypomorph and *pak3*^{e00329} is a milder loss-of-function allele.

Because *Exel9055* was not a deficiency and the two remaining alleles were hypomorphs, we created a deletion of *pak3* using the same method outlined in Parks *et al.* 2004 via FLP-mediated recombination between *pak3*^{d02472} and *pak3*^{e00329} (after backcrossing; see *Materials and Methods*).

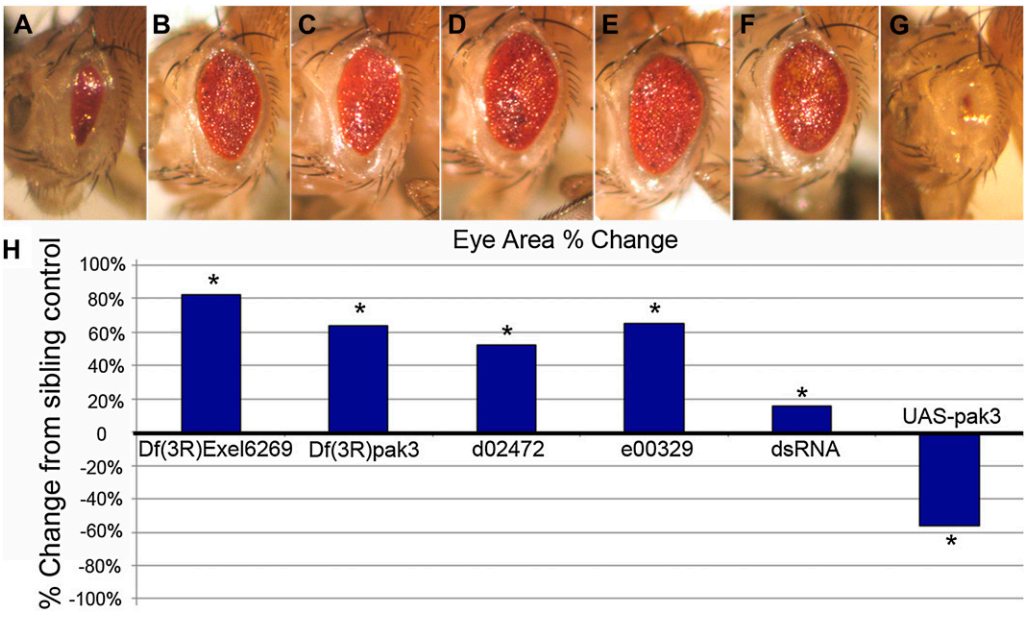

Figure 2 *pak3* alterations interacted strongly with *spastin* overexpression in the eye. (A) *GMR-Gal4/+*; *P{EP}spas*^{T32}/+ sibling controls show the amount of eye size reduction due to *spastin* overexpression. Eye area was compared with sibling controls in each cross due to variation in control eye size between genetic backgrounds. Both *Df(3R)Exel6269* (B) and *Df(3R)pak3* (C) partially rescued eye size and texture when in combination with *spastin* overexpression. Similarly, transposable element insertions, *pak3*^{d02472} (D) and *pak3*^{e00329} (E), and RNAi (VDRC 39844) knockdown of *pak3* (F) all showed suppression. Conversely, simultaneous overexpression of both *spastin* and *pak3* resulted in strong enhancement of the eye reduction (G). The eye area of each mutant genotype was measured, the area of its sibling control subtracted, and the difference expressed as the % change from the sibling control in H. Positive values represent suppression of eye reduction; negative values represent enhancement. The (*) marks a statistically significant difference from sibling controls as determined by Student's *t* test. The *P* value for dsRNA (in the absence of *Dicer2*) was 0.012, while for all other mutants $P < 0.005$.

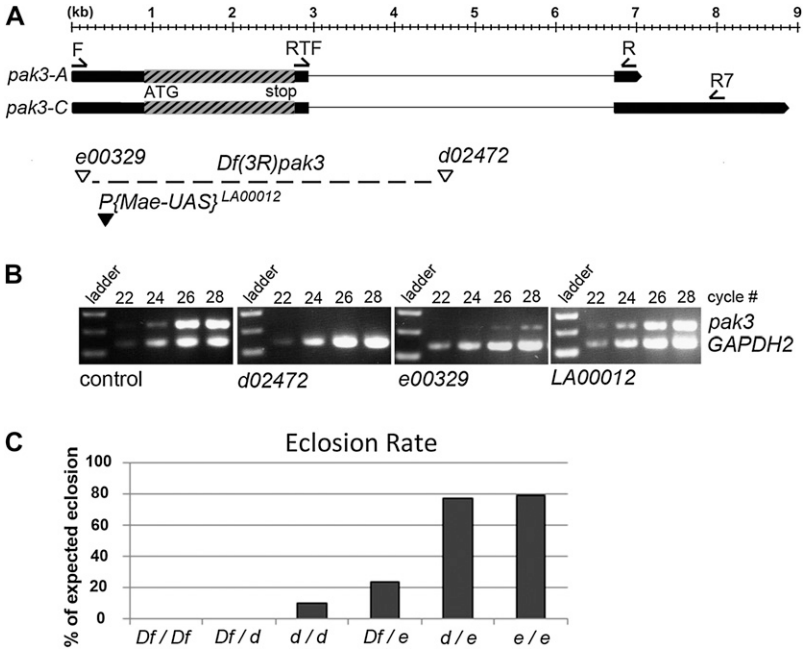

Figure 3 The molecular characterization of *pak3* alleles. (A) The *pak3* gene annotation predicted two primary transcripts, *pak3-A* and *pak3-C*, and our amplification experiments with the primers shown (indicated by half arrows; F, RTF, R, and R7) confirmed this prediction. The sites of PBac{RB} and P{XP} insertion are indicated by open triangles: $pak3^{e00329}$ is within the 5′-UTR and $pak3^{d02472}$ is within a portion of the intron that is conserved among 12 *Drosophila* species. The UAS insertion ($pak3^{LA00012}$) is indicated by a solid triangle in the 5′-UTR. (B) Semiquantitative RT-PCR revealed that $pak3^{d02472}$ homozygous larvae displayed severely reduced levels of *pak3*, and only after additional amplification cycles (35+) could transcript be visualized (not shown). Furthermore, *pak3* expression was reduced considerably, but not abolished, in $pak3^{e00329}$ larvae as compared to control larvae. Finally, the insertion of $pak3^{LA00012}$, although also within the 5′-UTR, did not disrupt *pak3* transcription levels. In all cases, *GAPDH2* was amplified simultaneously as a control for cDNA levels (141 bp). The *pak3* amplification shown was performed with the RTF and R primers in A, which resulted in a product of 228 bp. Products from progressive cycle numbers (22, 24, 26, and 28) were included to aid in determination of cDNA levels. (C) Deletion of *pak3* within the null allele, *Df(3R)pak3* (labeled "Df"), resulted in complete elimination of viable adult flies: in fact, homozygous embryos hatched but died as first instar larvae. *Df(3R)pak3*/$pak3^{d02472}$ also showed no pupal eclosion, but larvae developed to the third instar before dying. Consistent with the severity of reduced transcription of *pak3*, the hypomorphic alleles, $pak3^{d02472}$ (labeled "d") and $pak3^{e00329}$ (labeled "e") displayed reduced pupal eclosion rate. Only 11% of the expected $pak3^{d02472}$ homozygous adults emerged (χ^2, $P < 6E\text{-}54$), while 79% of the expected $pak3^{e00329}$ homozygotes eclosed (χ^2, $P < 0.003$). All other genetic combinations consistently fit the pattern of reduced transcript causing reduced viability.

This null allele, *Df(3R)pak3*, was confirmed by amplification of the hybrid element alone as well as the hybrid insertion with flanking genomic DNA in both 5′ and 3′ directions. Furthermore, RT-PCR of mRNA from *Df(3R)pak3* larvae showed complete loss of *pak3* transcript (data not shown).

pak3 is an essential gene

Since this is the first characterization of *pak3* mutant alleles, we determined whether reduction of *pak3* levels affects the development of healthy adult flies. Measurement of pupal eclosion rates showed that *pak3* reduction/loss decreased the number of homozygous adults, relative to the expected genetic ratio with heterozygous siblings. Consistent with the allelic severity in transcription levels, *Df(3R)pak3* homozygotes were completely lethal, and pupal eclosion rates were reduced more drastically in $pak3^{d02472}$ than $pak3^{e00329}$ flies (Figure 3C). $pak3^{d02472}$ homozygous adults emerged 10% as frequently as expected (χ^2 $P < 6E\text{-}54$), while $pak3^{e00329}$ homozygotes eclosed at nearly 80% of the expected rate (χ^2 $P < 0.003$). Transheterozygous genetic combinations followed the same trend: less *pak3* expression resulted in fewer healthy adults. We also established that *Df(3R)pak3/+* heterozygotes eclosed at a comparable rate to the sibling controls (data not shown), which indicates that *pak3* loss has no dominant effect on viability. Of the two lethal genotypes, *Df(3R)pak3* homozygotes developed to first instar larvae, whereas *Df(3R)pak3/*$pak3^{d02472}$ larvae matured to the third instar larval stage. Therefore, both transcriptional levels and animal viability supported an allelic series in which $pak3^{e00329}$ is of intermediate severity, $pak3^{d02472}$ is a strong loss-of-function allele, and *Df(3R)pak3* is a null. Furthermore, *pak3* is required for viability beyond the first instar larval stage.

pak3 plays a role with spastin in synapse formation

The genetic interaction of *pak3* with ectopic *spastin* in the eye was suggestive of a functional relationship. To test this possibility, we examined the genetic interaction between *spastin* and *pak3* at a site of known biological relevance to *spastin* function, the larval NMJ. Here, Spastin is required within neurons to remodel the microtubule cytoskeleton for proper synapse formation and branching (Sherwood *et al.* 2004). To evaluate the effects of combinatorial mutant genotypes on synapse morphology and microtubule distribution, we immunostained larval fillets with antibodies directed against horseradish peroxidase (HRP) and Futsch (Figure 4A). Anti-HRP labels the neuronal membrane, allowing quantification of the total number of synaptic boutons and the number of terminal boutons, a measure of synaptic arbor branching. Anti-Futsch (mAb 22C10) recognizes the *Drosophila* ortholog of MAP1b, revealing the integrity of the microtubule architecture within each terminal bouton. We also quantified the frequency of distal bouton "bunches," which we define as a collection of similarly sized boutons arranged in a grape-like cluster in which connections between boutons are difficult to discern (Figure 4B). Previously reported examples of additional small boutons at the distal tips of axons have been referred to as "satellite" or "supernumerary" boutons, but those are typically

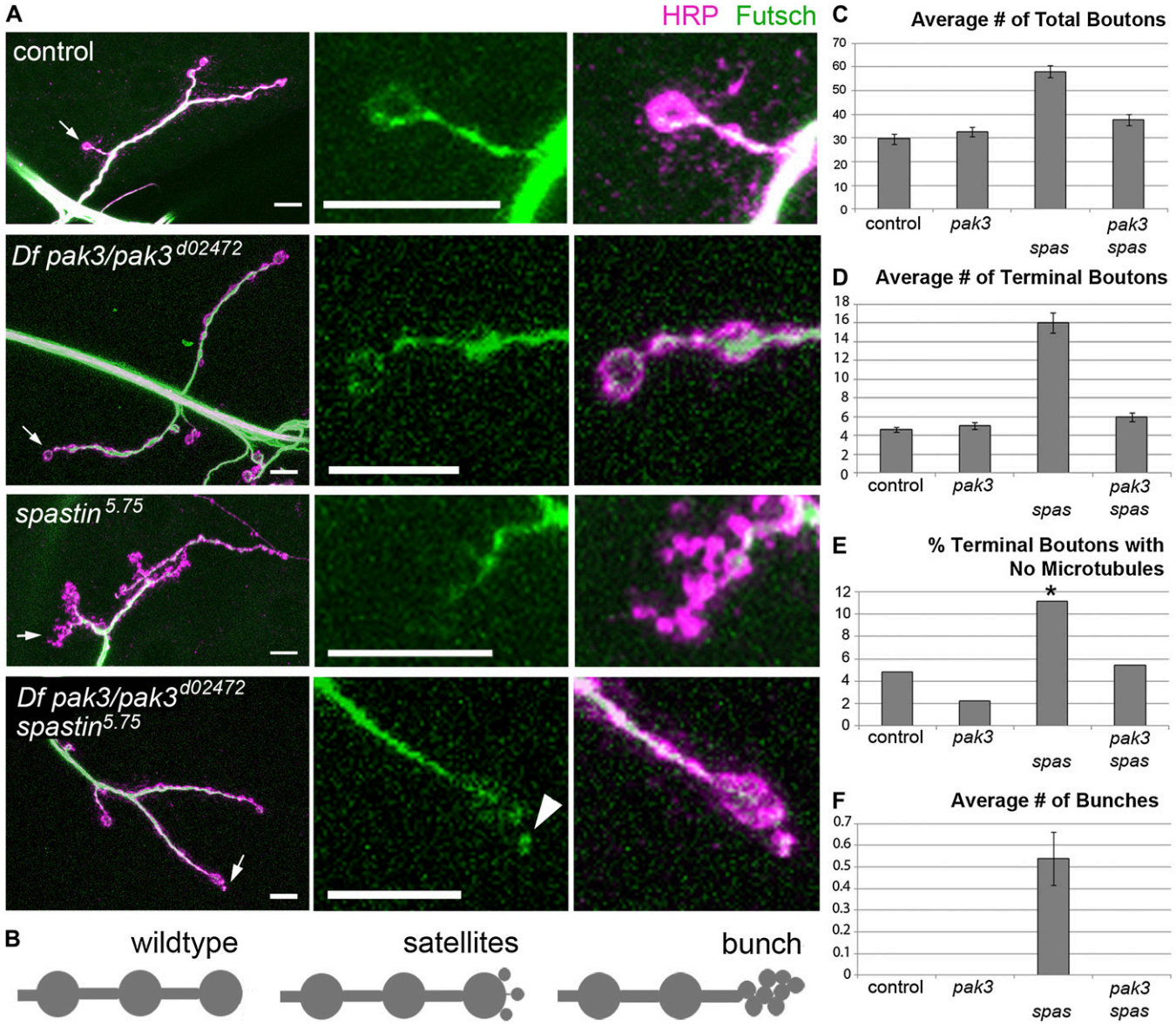

Figure 4 Reduction of *pak3* rescues the morphological defects induced by loss of *spastin* at the larval neuromuscular junction. (A) The larval NMJ at muscle 4 was stained with anti-HRP (magenta) to mark the neuronal membrane and with mAb 22C10 (green) to stain the microtubule-associated protein Futsch in neurons. Bar, 10 μm. White arrows indicate which terminus is enlarged. Enlarged views include a single axon terminus with anti-Futsch alone (middle column) or anti-Futsch, anti-HRP merged (right column). (B) Cartoons describing the typical round distal bouton (wild type), the small boutons (satellites) that bud from the distal tip in both wild-type and mutant NMJs, and the small similarly sized boutons that form a complex grape-like cluster (bunch) in *spastin* null mutants. (C–F) Characteristics of these neurons (*i.e.*, total bouton number, terminal bouton number, microtubule distribution, and grape-like bunches) are quantified in the graphs on the right. Error bars represent standard error. For the microtubule distribution graph, the asterisk indicates statistical significance from every other genotype (Student's *t* test, $P < 0.02$). In control animals, the synaptic boutons were linearly arranged and the microtubules were present in loops at the distal tips of each axonal branch. In *Df(3R)pak3/pak3*^{d02472} larvae, bouton number and structure were very similar to wild type in all categories. However, *spastin* null larvae demonstrated a dramatic increase in bouton number and a very highly disrupted bouton structure, including many bunches and a lack of distal microtubules. Interestingly, *pak3*, *spastin* double mutants formed boutons in a number and cluster structure more similar to *pak3* mutants, with microtubules present even in small terminal boutons (arrowhead). Results indicated that *pak3* loss alleviates some of the most severe phenotypes of *spastin* null animals, including the *spastin* null microtubule defects. This confirmed the genetic interaction between *spastin* and *pak3* and was consistent with a role for both in bouton formation or maintenance.

limited in number, with clear connections to the distal "mother" bouton, and are observed at a low level in wild-type neurons. By contrast, bunches are never seen in wild-type NMJs, and they represent a morphological hallmark of *spastin* mutations.

Compared to the NMJs of other larval muscles, motor neurons that synapse onto larval muscle 4 have simple arbors that lie on the muscle surface, making it ideal for morphological analysis. Muscle 4 is innervated by two separate excitatory, glutamatergic neurons, MN4-Ib (large bouton size)

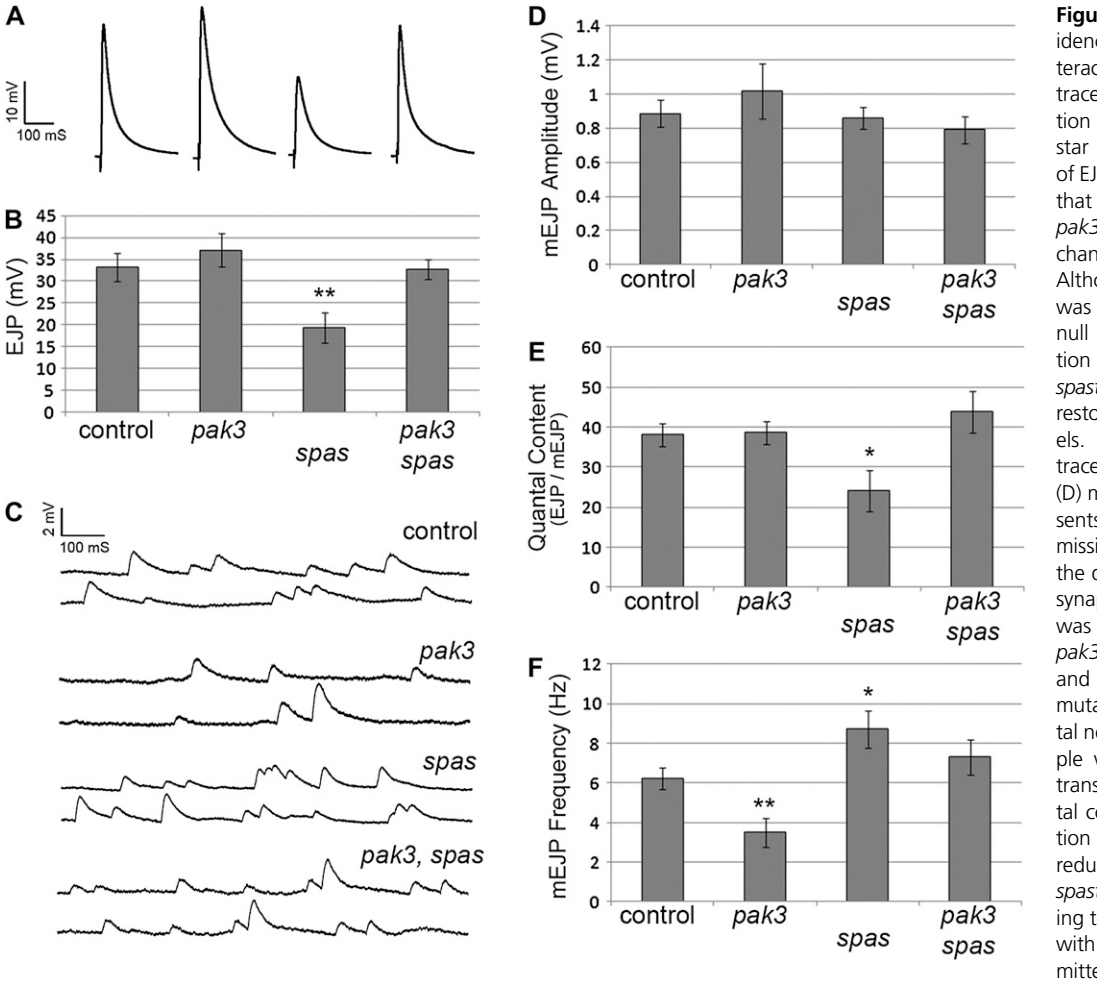

Figure 5 Electrophysiological evidence that *pak3* and *spastin* interact functionally. (A) Averaged traces of evoked excitatory junction potentials (EJPs) in third instar larvae. (B) Mean amplitude of EJPs (mV) ± SEM. EJPs showed that neuronal function of *Df(3R) pak3/pak3*^{d02472} larvae was unchanged from *w*^{1118} controls. Although neuronal signaling was impaired in *spastin*$^{5.75}$ null larvae, simultaneous reduction of *pak3* levels (*Df(3R)pak3 spastin*$^{5.75}$*/pak3*^{d02472} *spastin*$^{5.75}$) restored the EJPs to wild-type levels. (C) Miniature EJP (mEJP) traces from third instar larvae. (D) mEJP amplitude, which represents the amount of neurotransmission from a single vesicle and the density and function of postsynaptic glutamate receptors, was equivalent to wild type in *pak3* mutants, *spastin* mutants, and *pak3*, *spastin* double mutants. (E) The ratio of EJP (total neurotransmission from multiple vesicles)/mEJP (single vesicle transmission) approximates quantal content. Simultaneous reduction of *pak3* suppressed the reduction in quantal content in *spastin* null larvae, demonstrating that Pak3 acts presynaptically with Spastin in regulating transmitter release. (F) mEJP frequency (Hz) was reduced in *pak3* mutants alone, but slightly elevated in *spastin* null larvae. The *pak3*, *spas* double mutants displayed an intermediate mEJP frequency and did not statistically differ from wild type. *$P \leq 0.05$, **$P \leq 0.01$, by Student's *t* test.

and MNISN-Is (small bouton size) (Hoang and Chiba 2001). Wild-type synaptic boutons are arranged linearly, with relatively little branching (Figure 4A). The average number of boutons (Ib and Is) totaled ~30 and the number of terminal boutons averaged 4 per hemisegment (Figure 4, C and D). The neuronal microtubules extended throughout the axon and most formed a loop at the distal tip, indicating a static or stable bouton: <5% of distal boutons lacked microtubules (Figure 4E). Bunches of terminal boutons were never observed in wild-type neurons (Figure 4F). Although observation of third instar *Df(3R)pak3* homozygous nulls was not possible due to lethality, evaluation of *pak3*^{d02472} homozygotes and *Df(3R)pak3/pak3*^{d02472} transheterozygotes revealed that reduction of *pak3* only mildly affected synaptic bouton structure. *pak3* mutant larvae displayed linear bouton arrangements very similar to wild type (Figure 4), with little to no change in bouton number, size, morphology, or microtubule distribution.

With these characteristics as a baseline, we evaluated the effects of *pak3* mutation in a *spastin*$^{5.75}$ heterozygous background. On their own, *spastin* heterozygotes were moderately affected at the larval NMJ. While they displayed round, well-defined boutons in a linear array similar to wild type and to *pak3*^{d02472} mutants alone, distal microtubules were diffuse or absent twice as frequently as in wild type, and bouton bunches were observed. Removal of *pak3* from a *spastin* heterozygous background restored the number of bunches almost to wild-type levels, suggesting that Pak3 activity is required for the *spastin* mutant phenotype (supporting information, Figure S1).

Consistent with a genetic interaction between *pak3* and *spastin* at the synapse, loss of *pak3* in a *spastin*$^{5.75}$ homozygous background also alleviated the defects observed in *spastin*$^{5.75}$ homozygotes alone. *spastin* null larvae have severely increased numbers of boutons, mainly at the terminals of each branch, where bunches are prevalent. Microtubules in these boutons are diffuse at the distal tips and do not form the loops that are found in wild-type boutons. In animals lacking both *pak3* and *spastin*, these defects in axonal branching and microtubule organization were completely restored to wild type (Figure 4, C–E, Figure S1). Bunched synaptic boutons were also no longer observed

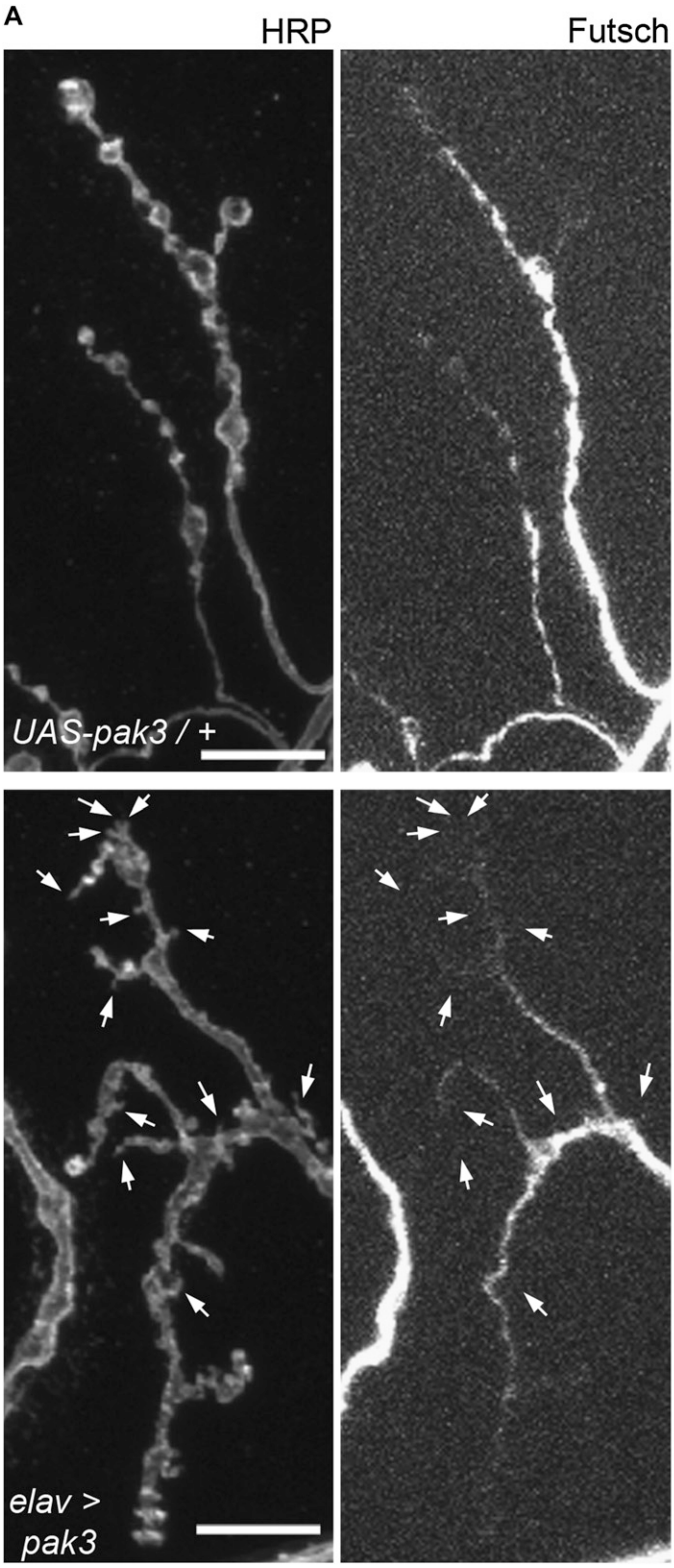

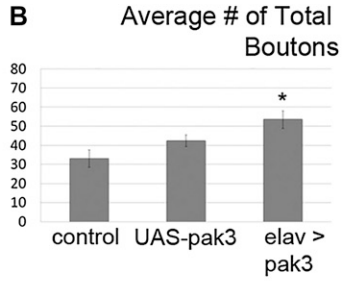

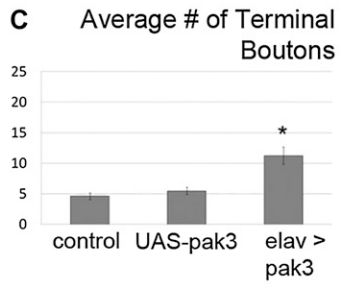

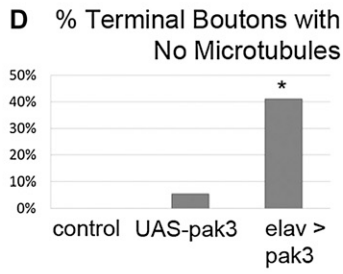

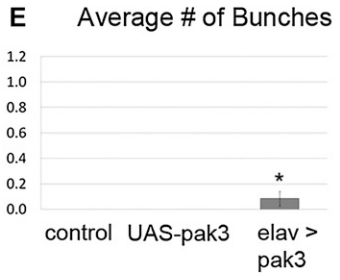

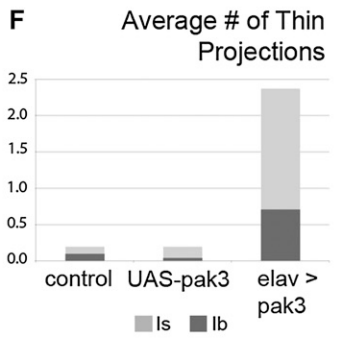

Figure 6 Overexpression of *pak3* in neurons results in increased thin projections and reduced microtubules. (A) Immunofluorescence marks neuronal membrane (anti-HRP) and microtubules (anti-Futsch) at the larval NMJ of muscle 4. Bar, 10 μm. The control genotype (top row) is *P{MaeUAS.6.11}pak3^{LA00012}*/+ and the overexpression genotype (bottom row) is *elav-Gal4*/+; *P{MaeUAS.6.11}pak3^{LA00012}*/+. (B–F) Quantification of bouton number, branching, microtubule defects, bouton clustering, and filopodial projection is shown in the set of graphs on the right. Error bars represent standard error and asterisks indicate statistical significance from controls (Student's *t* test, $P < 0.05$). Neuronal overexpression of *pak3* via *elav-Gal4* resulted in increased bouton number, branching, and dramatically reduced distal microtubule distribution. The morphology also displayed increased thin projections (arrows), which were morphologically distinct from bunches and generally lacked microtubules. The thin projections were included in the number of total and terminal boutons.

(Figure 4F), confirming a requirement for functional *pak3* in the establishment of these structures.

pak3 plays a role with spastin in synapse function

Strikingly, the suppression of *spastin* mutant effects also extended to synaptic function. We measured the electrophysiological response of body wall muscles to motor neuron stimulation at the NMJ and found that the evoked EJPs in *Df(3R)pak3/pak3^{d02472}* larvae were indistinguishable in magnitude from controls, consistent with the wild-type synaptic bouton number and arrangement in *pak3* mutants. In contrast, EJPs are dramatically reduced in *spastin$^{5.75}$* larvae,

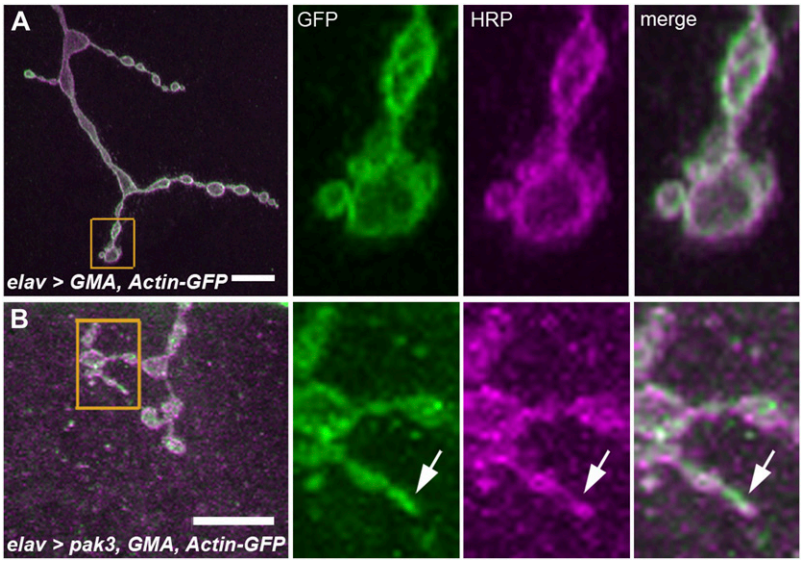

Figure 7 Actin is present in *pak3*-induced filopodia-like projections. (A and B) GFP (green), HRP (magenta). Bar, 10 μm. Orange boxes are enlarged in the last three panels. (A) *w*; *UAS-Act5c:GFP*/+; *elav-Gal4*, *UAS-GMA*/+. (B) *w*; *elav-Gal4*/*UAS-Act5c:GFP*; *UAS-pak3*^{LA00012}/*UAS-GMA*. Actin is found in the projections of *pak3* overexpressing neurons (white arrows). Of 15 filopodia in controls, and 32 filopodia in *pak3* overexpressing neurons, 100% were positive for actin.

correlating with their altered synapse morphology and microtubule distribution (Figure 5 and Sherwood *et al.* 2004). However, in larvae simultaneously lacking *pak3* and *spastin*$^{5.75}$, EJP amplitudes were indistinguishable from controls, reminiscent of the morphological suppression (Figure 5, Figure S2). Examination of spontaneously occurring, miniature EJP (mEJP) amplitudes revealed that these effects on evoked postsynaptic responses were due to alterations in quantal content, a measure of the number of neurotransmitter vesicles released following an action potential. Quantal content was unaffected by *pak3* reduction alone, significantly reduced in *spastin* mutants, and restored to control levels when both proteins were simultaneously reduced. Therefore, *pak3* loss of function completely suppresses defects in microtubule distribution, synapse morphology, and synaptic function in *spastin* mutant larvae.

pak3 overexpression in neurons induces filopodial projections

Given that loss of *pak3* was able to reorganize or restore neuromuscular junction morphology in *spastin* mutants, we investigated the consequences of *pak3* overexpression at the NMJ to better understand its function (Figure 6). Similar to *spastin* mutants, overexpression of *pak3* in neurons via the *elav-Gal4* driver reduced microtubules in terminal synaptic boutons. Neuronally overexpressed Pak3 also significantly increased the amount of branching at the NMJ. However, these branches resembled filopodial projections, rather than the synaptic bouton bunches observed in *spastin* mutants. Projections caused by neuronal overexpression of Pak3 were found frequently in type Is neurons (17-fold increase compared to controls) as well as type Ib (11-fold more), and were morphologically unlike any of our previous phenotypes.

As overexpression of *pak3* has been shown in cell culture to induce actin-mediated filopodia formation, the observation of similar thin projections in neurons overexpressing *pak3* led us to evaluate neuronal F-actin distribution. Using *elav-Gal4*, we simultaneously drove neuronal expression of Pak3 with the fluorescently tagged actin-binding domain of moesin in combination with fluorescently tagged actin (Edwards *et al.* 1997; Verkhusha *et al.* 1999). The GFP-moesin fragment and GFP-actin were utilized together to maximize the signal while minimizing the amount of exogenous actin expression. Using this method, we confirmed that 100% of *pak3*-induced filopodia were actin-rich (Figure 7, control $n = 15$ filopodia, *pak3* overexpression $n = 32$).

To determine whether these filopodial projections induced by neuronal *pak3* overexpression were functional synapses, we immunostained larvae using antibodies to the presynaptic proteins synapsin (Syn) and Brüchpilot (Brp), and to the postsynaptic proteins Discs-large (Dlg) and glutamate receptor IIA (GluR) (Figure 8). Syn is a regulator of neurotransmitter vesicle release, and Brp marks presynaptic active zones. Dlg is a component of the muscle subsynaptic reticulum that surrounds the neuronal membrane at wild-type synapses, and GluR is a neurotransmitter receptor. While neurons expressing exogenous *pak3* displayed Syn expression to the edges of all protrusions (Figure 8, A and D) and frequently contained Brp punctae (34% of 32 filopodia, data not shown), there was not corresponding Dlg staining surrounding the axonal extensions (Figure 8, B and E), nor were glutamate receptors present (Figure 8, C and F). Generally, long, thin projections did not include Brp staining (83% Brp^{-}), while shorter, thicker projections were much more likely to show synaptic vesicle staining (88% Brp^{+}). The projections induced by Pak3 overexpression were thus not stable synapses but dynamic and developing structures, consistent with their filopodial morphology.

Taken together, our data suggest that wild-type Pak3 functions *in vivo* to promote filopodia formation during synapse development. While *pak3* mutation is not deleterious to the overall morphology and basal function of larval NMJ synapses, in the background of *spastin* mutations *pak3* loss

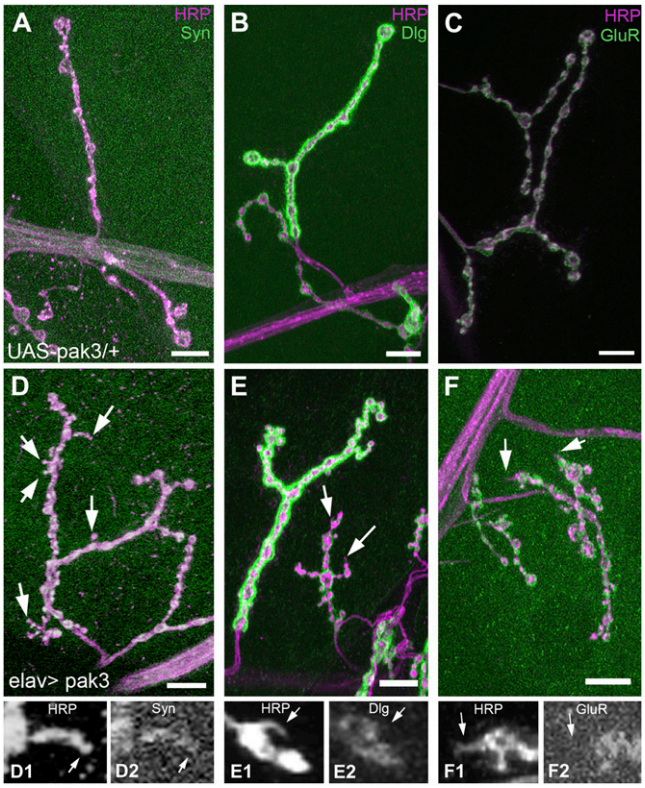

Figure 8 Thin axonal projections, induced by neuronal overexpression of *pak3*, display presynaptic, but not postsynaptic markers. (A and D) HRP (magenta), synapsin (Syn) (green). (B and E) HRP (magenta), Discs-large (Dlg) (green). (C and F) HRP (magenta), GluR IIA (green). (A–F) Bar, 10 μm. (A–C) *UAS-pak3*^{LA00012}/+ larvae. (D–F) *elav-Gal4*/+; *UAS-pak3*^{LA00012}/+ larvae. (A) Syn, a presynaptic protein, is found throughout wild-type boutons. (B) Dlg, a postsynaptic marker, shows fluorescence surrounding each wild-type bouton where the neuron meets the muscle. (C) GluR is also found postsynaptically in wild-type controls. (D) Syn is present even in the thin protrusions caused by neuronal *pak3* overexpression (large white arrows). (E) However, the axonal extensions induced by exogenous *pak3* do not have surrounding Dlg staining (large white arrows), F) nor do they show GluR (large white arrows). In each case, a single projection is enlarged below (HRP: D1, E1, and F1) and the presence of Syn (D2) or absence of Dlg (E2) and GluR (F2) is indicated (small white arrow).

has a dramatic effect, providing complete suppression of *spastin* mutant phenotypes.

Discussion

Using an unbiased deletion screen, we have identified the p21-activated kinase *pak3* as a potent genetic regulator of *spastin* function. Only 4% of deficiency chromosomes (of the genome-spanning collection of 400 lines used in this study) suppressed *spastin* overexpression as strongly as *pak3*, providing further evidence of a significant relationship between it and *spastin*.

Our initial screen showed that reduction of *pak3* suppresses the small eye produced by *spastin* overexpression, while simultaneous overexpression of *pak3* and *spastin* enhances the eye phenotype. In this tissue, then, *pak3* appears to positively regulate *spastin* function. However, at the larval neuromuscular junction, a known site of *spastin* action (Sherwood *et al.* 2004; Orso *et al.* 2005), we found that reduction of *pak3* transcript suppresses both the abnormal, bunched morphology and sparse microtubules of synaptic boutons caused by *spastin* loss. Remarkably, this was also sufficient to restore neuronal function, such that the synaptic physiology at the NMJ of *pak3*, *spastin* double mutants is indistinguishable from wild-type animals.

That *pak3* reduction suppresses the effects of both *spastin* overexpression (in the eye) and *spastin* reduction (at the NMJ) has several possible implications. *pak3* and *spastin* may serve different functions within different tissues, acting antagonistically at the larval NMJ but synergistically within the eye. Alternatively, because disruption of *spastin* levels in either direction results in microtubule loss (Sherwood *et al.* 2004), *pak3* may suppress the effects of this loss in each tissue. A third possibility is that eye size reduction may not be representative of the directionality of microtubule effects. Overexpression of the microtubule-protecting protein Tau (Yu *et al.* 2008), for example, also causes a reduced eye phenotype in *Drosophila* (Jackson *et al.* 2002), although it has opposing effects on the stability of the microtubule network compared to Spastin. The fact that eye reduction may occur in either case precludes clear interpretation about a protein's effects on the microtubule cytoskeleton based on the direction of the genetic interaction. What is clear, however, is that because *pak3* mutation alters synapse function, morphology, and microtubule architecture in *spastin* nulls, Pak3 must not regulate Spastin directly to affect these changes. Rather, the two proteins must act in parallel to regulate synaptic development.

Furthermore, the synaptic functions of each are distinct. Loss of *spastin* reduces the distal microtubule network and causes bunched synaptic boutons, enhancing spontaneous neurotransmitter release slightly, but reducing action potential-evoked neurotransmitter release. In contrast, *pak3* loss compromises the frequency of spontaneous neurotransmitter release, supporting a role for Pak3 in presynaptic function, but does not affect single evoked potentials. It also has no direct effect on neuronal microtubules or synapse morphology. Bunched morphology boutons are never present in *pak3* mutants and are in fact decreased by the simultaneous reduction of *pak3* and *spastin*. The formation of bunches therefore requires not only *spastin* reduction, but also functional *pak3* activity.

Members of the Pak protein family have been implicated in regulation of both the actin and the microtubule networks. Our results suggest that the increase in filopodia induced by *pak3* overexpression in cell culture (Asano *et al.* 2009) also occurs *in vivo*, providing further support for Pak3-mediated regulation of the actin cytoskeleton. In cultured mammalian cells, Rac or Cdc42 activation not only leads to changes in actin polymerization, but also induces phosphorylation of Stathmin by Pak1, inactivating Stathmin's microtubule-destabilizing activity (Daub *et al.* 2001). Stathmin similarly disrupts the microtubule network in flies and is required during CNS and PNS development (Ozon *et al.* 2002),

suggesting the possibility that Pak3 regulates the neuronal microtubule cytoskeleton through a similar pathway.

In summary, we have shown that *pak3*, which encodes an actin-regulatory protein, promotes filopodia formation *in vivo* and affects spontaneous neurotransmitter release in developing synapses. *pak3* exhibits a remarkable genetic interaction with *spastin* at the larval NMJ, suppressing the morphological and functional defects characteristic of *spastin* mutants when it is also reduced. The *spastin*-antagonizing function of *pak3* may occur because of, or in addition to, its role in regulating the actin cytoskeleton. Given the significant parallels between Spastin function in *Drosophila* and humans, it will be important to investigate the mammalian Pak proteins as potential therapeutic targets in AD-HSP.

Acknowledgments

We gratefully acknowledge Fang Du for excellent technical assistance with larval fillets as well as Daniel Marchuk and Pradeep Bugga for help with the deficiency screen. Many thanks to Kai Zinn, in whose laboratory this screen was initiated, David Sherwood, Dan Tracey, Amy Bejsovec, and the rest of the NTS lab for critical discussions. We are also grateful to Doug Marchuk, Vann Bennett, and the Department of Molecular Genetics and Microbiology for their invaluable support and the Bloomington, Kyoto, Vienna, and Harvard stock centers for provision of fly lines. NTS received funding from the National Institute of Neurological Disorders and Stroke (NINDS) (RO1NS63896), the Spastic Paraplegia Foundation, and the Duke University Institute for Genome Sciences and Policy (IGSP). E.F.O. was funded by postdoctoral fellowships from the IGSP and the Ruth K. Broad Biomedical Research Foundation. H.B. and B.Z. were supported by a grant from NINDS (RO1NS06878).

Literature Cited

Albin, S. D., and G. W. Davis, 2004 Coordinating structural and functional synapse development: postsynaptic p21-activated kinase independently specifies glutamate receptor abundance and postsynaptic morphology. J. Neurosci. 24: 6871–6879.

Ang, L. H., J. Kim, V. Stepensky, and H. Hing, 2003 Dock and Pak regulate olfactory axon pathfinding in Drosophila. Development 130: 1307–1316.

Asano, Y., A. Jimenez-Dalmaroni, T. B. Liverpool, M. C. Marchetti, L. Giomi *et al.*, 2009 Pak3 inhibits local actin filament formation to regulate global cell polarity. HFSP J. 3: 194–203.

Bahri, S. M., J. M. Choy, E. Manser, L. Lim, and X. Yang, 2009 The Drosophila homologue of Arf-GAP GIT1, dGIT, is required for proper muscle morphogenesis and guidance during embryogenesis. Dev. Biol. 325: 15–23.

Bao, H., R. W. Daniels, G. T. MacLeod, M. P. Charlton, H. L. Atwood *et al.*, 2005 AP180 maintains the distribution of synaptic and vesicle proteins in the nerve terminal and indirectly regulates the efficacy of Ca2+-triggered exocytosis. J. Neurophysiol. 94: 1888–1903.

Bokoch, G. M., 2003 Biology of the p21-activated kinases. Annu. Rev. Biochem. 72: 743–781.

Chinnery, P. F., S. M. Keers, M. J. Holden, V. Ramesh, and A. Dalton, 2004 Infantile hereditary spastic paraparesis due to codominant mutations in the spastin gene. Neurology 63: 710–712.

Conder, R., H. Yu, M. Ricos, H. Hing, W. Chia *et al.*, 2004 dPak is required for integrity of the leading edge cytoskeleton during Drosophila dorsal closure but does not signal through the JNK cascade. Dev. Biol. 276: 378–390.

Conder, R., H. Yu, B. Zahedi, and N. Harden, 2007 The serine/threonine kinase dPak is required for polarized assembly of F-actin bundles and apical-basal polarity in the Drosophila follicular epithelium. Dev. Biol. 305: 470–482.

Daub, H., K. Gevaert, J. Vandekerckhove, A. Sobel, and A. Hall, 2001 Rac/Cdc42 and p65PAK regulate the microtubule-destabilizing protein stathmin through phosphorylation at serine 16. J. Biol. Chem. 276: 1677–1680.

Dietzl, G., D. Chen, F. Schnorrer, K. C. Su, Y. Barinova *et al.*, 2007 A genome-wide transgenic RNAi library for conditional gene inactivation in Drosophila. Nature 448: 151–156.

Du, F., E. F. Ozdowski, I. K. Kotowski, D. A. Marchuk, and N. T. Sherwood, 2010 Functional conservation of human Spastin in a Drosophila model of autosomal dominant-hereditary spastic paraplegia. Hum. Mol. Genet. 19: 1883–1896.

Edwards, K. A., M. Demsky, R. A. Montague, N. Weymouth, and D. P. Kiehart, 1997 GFP-moesin illuminates actin cytoskeleton dynamics in living tissue and demonstrates cell shape changes during morphogenesis in Drosophila. Dev. Biol. 191: 103–117.

Errico, A., A. Ballabio, and E. I. Rugarli, 2002 Spastin, the protein mutated in autosomal dominant hereditary spastic paraplegia, is involved in microtubule dynamics. Hum. Mol. Genet. 11: 153–163.

Errico, A., P. Claudiani, M. D'Addio, and E. I. Rugarli, 2004 Spastin interacts with the centrosomal protein NA14, and is enriched in the spindle pole, the midbody and the distal axon. Hum. Mol. Genet. 13: 2121–2132.

Evans, K., C. Keller, K. Pavur, K. Glasgow, B. Conn *et al.*, 2006 Interaction of two hereditary spastic paraplegia gene products, spastin and atlastin, suggests a common pathway for axonal maintenance. Proc. Natl. Acad. Sci. USA 103: 10666–10671.

Fink, J. K., T. Heiman-Patterson, T. Bird, F. Cambi, M. P. Dube *et al.*, 1996 Hereditary spastic paraplegia: advances in genetic research. Hereditary Spastic Paraplegia Working group. Neurology 46: 1507–1514.

Gho, M., 1994 Voltage-clamp analysis of gap junctions between embryonic muscles in Drosophila. J. Physiol. 481(Pt 2): 371–383.

Hazan, J., N. Fonknechten, D. Mavel, C. Paternotte, D. Samson *et al.*, 1999 Spastin, a new AAA protein, is altered in the most frequent form of autosomal dominant spastic paraplegia. Nat. Genet. 23: 296–303.

Hing, H., J. Xiao, N. Harden, L. Lim, and S. L. Zipursky, 1999 Pak functions downstream of Dock to regulate photoreceptor axon guidance in Drosophila. Cell 97: 853–863.

Hoang, B., and A. Chiba, 2001 Single-cell analysis of Drosophila larval neuromuscular synapses. Dev. Biol. 229: 55–70.

Jackson, G. R., M. Wiedau-Pazos, T. K. Sang, N. Wagle, C. A. Brown *et al.*, 2002 Human wild-type tau interacts with wingless pathway components and produces neurofibrillary pathology in Drosophila. Neuron 34: 509–519.

Jaffer, Z. M., and J. Chernoff, 2002 p21-activated kinases: three more join the Pak. Int. J. Biochem. Cell Biol. 34: 713–717.

Jan, L. Y., and Y. N. Jan, 1976 Properties of the larval neuromuscular junction in Drosophila melanogaster. J. Physiol. 262: 189–214.

Kammermeier, L., J. Spring, M. Stierwald, J. M. Burgunder, and H. Reichert, 2003 Identification of the Drosophila melanogaster

homolog of the human spastin gene. Dev. Genes Evol. 213: 412–415.

Mannan, A. U., J. Boehm, S. M. Sauter, A. Rauber, P. C. Byrne *et al.*, 2006a Spastin, the most commonly mutated protein in hereditary spastic paraplegia interacts with Reticulon 1 an endoplasmic reticulum protein. Neurogenetics 7: 93–103.

Mannan, A. U., P. Krawen, S. M. Sauter, J. Boehm, A. Chronowska *et al.*, 2006b ZFYVE27 (SPG33), a novel spastin-binding protein, is mutated in hereditary spastic paraplegia. Am. J. Hum. Genet. 79: 351–357.

McDermott, C. J., C. E. Burness, J. Kirby, L. E. Cox, D. G. Rao *et al.*, 2006 Clinical features of hereditary spastic paraplegia due to spastin mutation. Neurology 67: 45–51.

Melzig, J., K. H. Rein, U. Schafer, H. Pfister, H. Jackle *et al.*, 1998 A protein related to p21-activated kinase (PAK) that is involved in neurogenesis in the Drosophila adult central nervous system. Curr. Biol. 8: 1223–1226.

Mentzel, B., and T. Raabe, 2005 Phylogenetic and structural analysis of the Drosophila melanogaster p21-activated kinase DmPAK3. Gene 349: 25–33.

Mentzel, B., E. Jauch, and T. Raabe, 2009 CK2beta interacts with and regulates p21-activated kinases in Drosophila. Biochem. Biophys. Res. Commun. 379: 637–642.

Menzel, N., D. Schneeberger, and T. Raabe, 2007 The Drosophila p21 activated kinase Mbt regulates the actin cytoskeleton and adherens junctions to control photoreceptor cell morphogenesis. Mech. Dev. 124: 78–90.

Naimi, M., S. Tardieu, C. Depienne, M. Ruberg, A. Brice *et al.*, 2005 Detection of genomic rearrangements by DHPLC: a prospective study of 90 patients with inherited peripheral neuropathies associated with 17p11.2 rearrangements. Am. J. Med. Genet. A 136: 136–139.

Newsome, T. P., S. Schmidt, G. Dietzl, K. Keleman, B. Asling *et al.*, 2000 Trio combines with dock to regulate Pak activity during photoreceptor axon pathfinding in Drosophila. Cell 101: 283–294.

Orso, G., A. Martinuzzi, M. G. Rossetto, E. Sartori, M. Feany *et al.*, 2005 Disease-related phenotypes in a Drosophila model of hereditary spastic paraplegia are ameliorated by treatment with vinblastine. J. Clin. Invest. 115: 3026–3034.

Ozon, S., A. Guichet, O. Gavet, S. Roth, and A. Sobel, 2002 Drosophila stathmin: a microtubule-destabilizing factor involved in nervous system formation. Mol. Biol. Cell 13: 698–710.

Parks, A. L., K. R. Cook, M. Belvin, N. A. Dompe, R. Fawcett *et al.*, 2004 Systematic generation of high-resolution deletion coverage of the Drosophila melanogaster genome. Nat. Genet. 36: 288–292.

Reid, E., M. Kloos, A. Ashley-Koch, L. Hughes, S. Bevan *et al.*, 2002 A kinesin heavy chain (KIF5A) mutation in hereditary spastic paraplegia (SPG10). Am. J. Hum. Genet. 71: 1189–1194.

Reid, E., J. Connell, T. L. Edwards, S. Duley, S. E. Brown *et al.*, 2005 The hereditary spastic paraplegia protein spastin interacts with the ESCRT-III complex-associated endosomal protein CHMP1B. Hum. Mol. Genet. 14: 19–38.

Roll-Mecak, A., and R. D. Vale, 2005 The Drosophila homologue of the hereditary spastic paraplegia protein, spastin, severs and disassembles microtubules. Curr. Biol. 15: 650–655.

Sanderson, C. M., J. W. Connell, T. L. Edwards, N. A. Bright, S. Duley *et al.*, 2006 Spastin and atlastin, two proteins mutated in autosomal-dominant hereditary spastic paraplegia, are binding partners. Hum. Mol. Genet. 15: 307–318.

Schickel, J., T. Pamminger, A. Ehrsam, S. Munch, X. Huang *et al.*, 2007 Isoform-specific increase of spastin stability by N-terminal missense variants including intragenic modifiers of SPG4 hereditary spastic paraplegia. Eur. J. Neurol. 14: 1322–1328.

Schneeberger, D., and T. Raabe, 2003 Mbt, a Drosophila PAK protein, combines with Cdc42 to regulate photoreceptor cell morphogenesis. Development 130: 427–437.

Sherwood, N. T., Q. Sun, M. Xue, B. Zhang, and K. Zinn, 2004 Drosophila spastin regulates synaptic microtubule networks and is required for normal motor function. PLoS Biol. 2: e429.

Stamer, K., R. Vogel, E. Thies, E. Mandelkow, and E. M. Mandelkow, 2002 Tau blocks traffic of organelles, neurofilaments, and APP vesicles in neurons and enhances oxidative stress. J. Cell Biol. 156: 1051–1063.

Stewart, B. A., H. L. Atwood, J. J. Renger, J. Wang, and C. F. Wu, 1994 Improved stability of Drosophila larval neuromuscular preparations in haemolymph-like physiological solutions. J. Comp. Physiol. A Neuroethol. Sens. Neural Behav. Physiol. 175: 179–191.

Svenson, I. K., M. T. Kloos, P. C. Gaskell, M. A. Nance, J. Y. Garbern *et al.*, 2004 Intragenic modifiers of hereditary spastic paraplegia due to spastin gene mutations. Neurogenetics 5: 157–164.

Thibault, S. T., M. A. Singer, W. Y. Miyazaki, B. Milash, N. A. Dompe *et al.*, 2004 A complementary transposon tool kit for Drosophila melanogaster using P and piggyBac. Nat. Genet. 36: 283–287.

Thomas, B. J., and D. A. Wassarman, 1999 A fly's eye view of biology. Trends Genet. 15: 184–190.

Tweedie, S., M. Ashburner, K. Falls, P. Leyland, P. McQuilton *et al.*, 2009 FlyBase: enhancing Drosophila Gene Ontology annotations. Nucleic Acids Res. 37: D555–D559.

Verkhusha, V. V., S. Tsukita, and H. Oda, 1999 Actin dynamics in lamellipodia of migrating border cells in the Drosophila ovary revealed by a GFP-actin fusion protein. FEBS Lett. 445: 395–401.

Wade, R. H., 2009 On and around microtubules: an overview. Mol. Biotechnol. 43: 177–191.

Warita, H., Y. Itoyama, and K. Abe, 1999 Selective impairment of fast anterograde axonal transport in the peripheral nerves of asymptomatic transgenic mice with a G93A mutant SOD1 gene. Brain Res. 819: 120–131.

Yu, W., L. Qiang, J. M. Solowska, A. Karabay, S. Korulu *et al.*, 2008 The microtubule-severing proteins spastin and katanin participate differently in the formation of axonal branches. Mol. Biol. Cell 19: 1485–1498.

Zhang, B., Y. H. Koh, R. B. Beckstead, V. Budnik, B. Ganetzky *et al.*, 1998 Synaptic vesicle size and number are regulated by a clathrin adaptor protein required for endocytosis. Neuron 21: 1465–1475.

Communicating editor: M. Nonet

GENETICS

Supporting Information
http://www.genetics.org/content/suppl/2011/06/24/genetics.111.130831.DC1

Loss of *Drosophila melanogaster p21-activated kinase 3* Suppresses Defects in Synapse Structure and Function Caused by *spastin* Mutations

Emily F. Ozdowski, Sophia Gayle, Hong Bao, Bing Zhang, and Nina T. Sherwood

DOI: 10.1534/genetics.111.130831

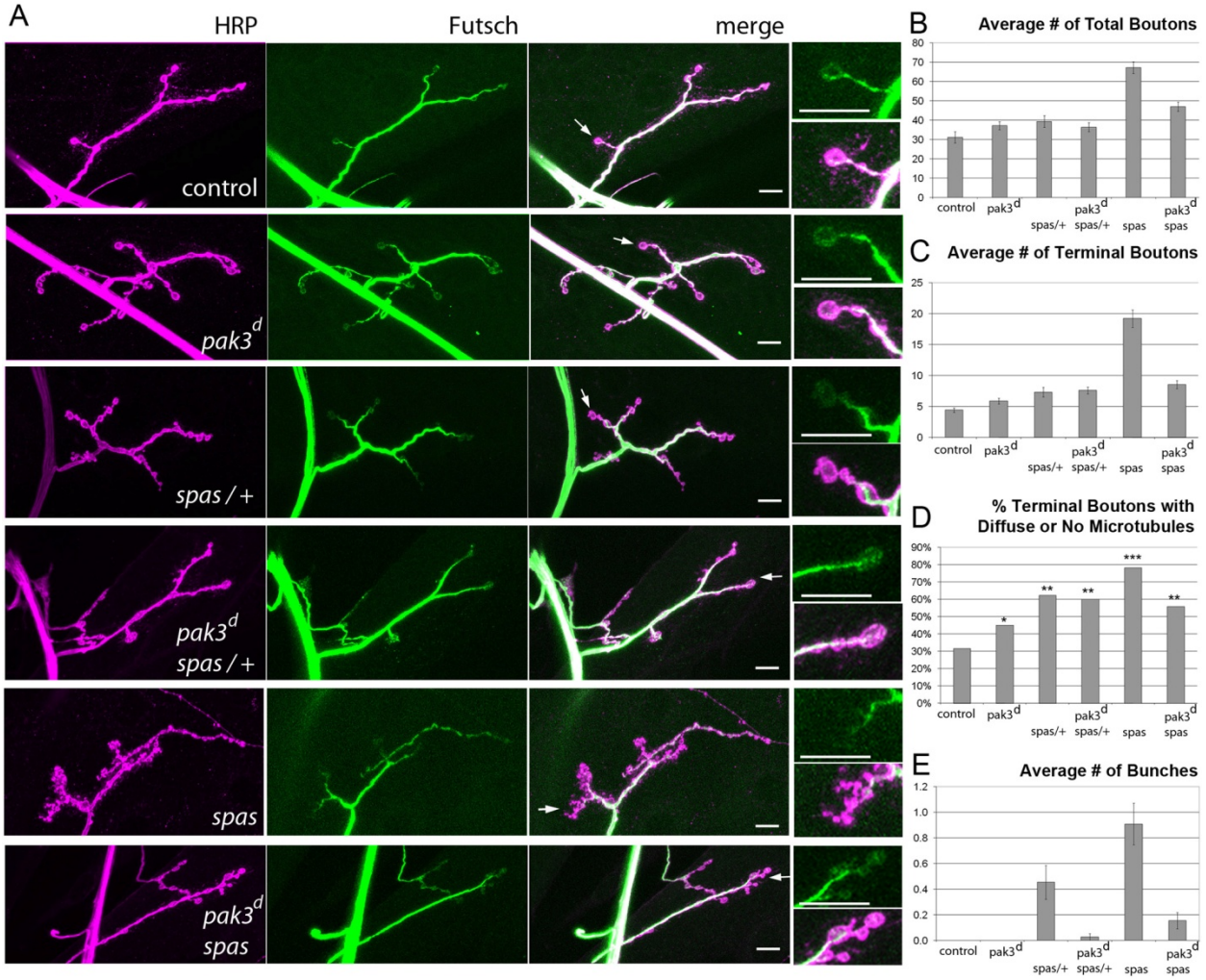

Figure S1 Restoration of *spastin* null synaptic bouton morphology is achieved by *pak3*^{d02472} homozygous hypomorphs similarly to *Df(3R)pak3* / *pak3*^{d02472} transheterozygotes. To diminish the impact of genetic background, we used transheterozygotes (labeled *pak3*^{d} here) of the backcrossed chromosome (*pak3*^{d02472}) and the original chromosome (*pak3*^{d02472*}), or their corresponding recombinant chromosomes with *spastin*$^{5.75}$ (For *spastin* heterozygous background: *pak3*^{d02472} *spastin*$^{5.75}$/ *pak3*^{d02472*} +; For double homozygotes: *pak3*^{d02472} *spastin*$^{5.75}$/ *pak3*^{d02472*} *spastin*$^{5.75}$). A) The larval NMJ at muscle 4 was stained with HRP (magenta) to mark the neuronal membrane and with 22C10 (green) to stain a microtubule-associated protein (Futsch) in neurons. Scale bar equals 10μm. White arrows (in merge column) indicate which terminus is enlarged on the right. Enlarged views include a single axon terminus with Futsch staining (top) or Futsch, HRP merged (bottom). B-F) Characteristics of these neurons (i.e. total bouton number, terminal bouton number, microtubule distribution, and grape-like bunches) are quantified in the graphs on the right. Error bars represent standard error. For the microtubule distribution graph, mutant genotypes were compared to wild-type and the Wilcoxon signed rank test measured significant differences: three classes, indicated by single (*), double (**), or triple (***) asterisks, differed from wild-type and from each other class. Three genotypes marked with double asterisks did not differ from each other and comprised one class. In control animals, the synaptic boutons were linearly arranged and the microtubules were present in loops at the distal tips of each axonal branch. In *pak3*^{d02472} / *pak3*^{d02472*} larvae, bouton number and structure were very similar to controls, with a slight increase in the loss of microtubules. Bouton numbers in *spastin*$^{5.75}$ heterozygotes were mostly wild-type as well, although there was an increase in bunches and terminal boutons lacking intact microtubules. However, axons with the combination of *pak3* and *spastin* mutations displayed far fewer bunches, reducing the number to almost control levels. This confirmed the genetic interaction between *spastin* and *pak3* and was consistent with a role for both in bouton formation or maintenance. *spastin* null larvae demonstrated a dramatic increase in bouton number and a very highly disrupted bouton structure including many bunches. Interestingly, *pak3*^{d02472}, *spastin*$^{5.75}$ double homozygotes formed boutons in a number and cluster structure more similar to *pak3* mutants, which indicated that *pak3* alleviates some of the most severe phenotypes of *spastin* null animals. Even the *spas* null microtubule defects were rescued by loss of *pak3*. Reducing *pak3* levels in multiple genetic combinations suppresses the *spastin* phenotype.

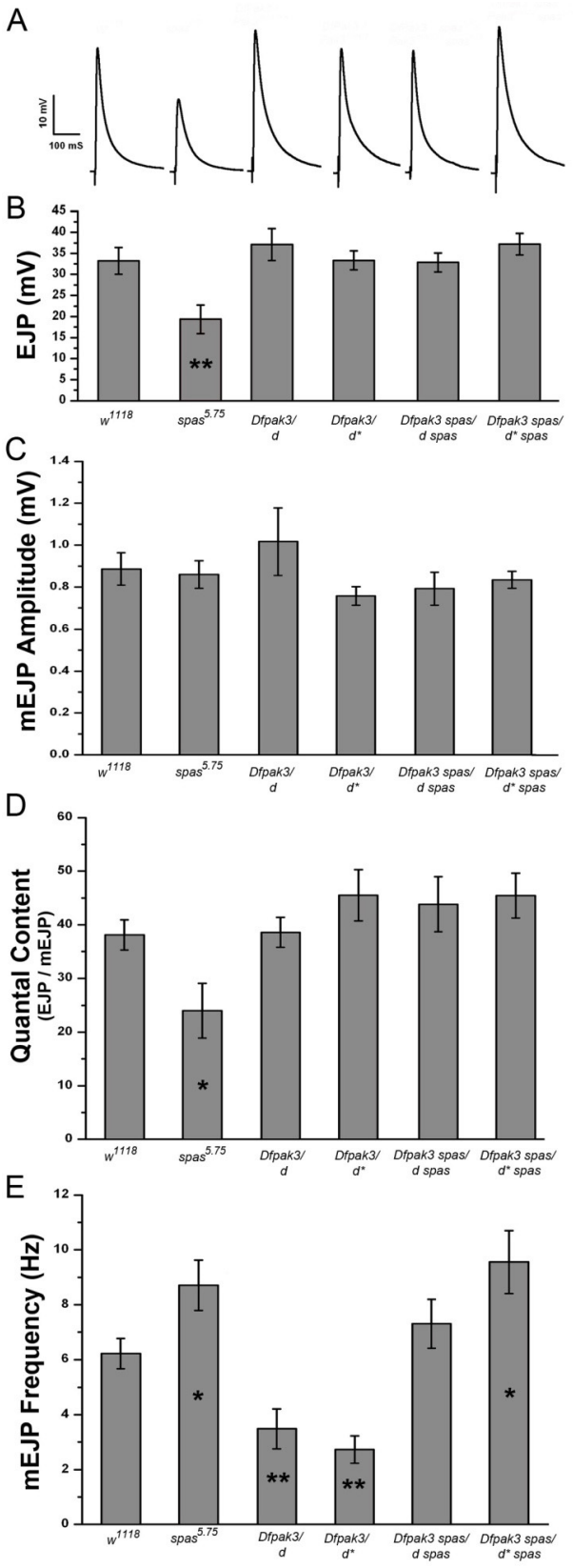

Figure S2 Presynaptic signaling is similar between *Df(3R)pak3*/ $pak3^{d02472}$ and *Df(3R)pak3*/ $pak3^{d02472*}$, and each restores *spastin* defective neurotransmission. In each panel, (*) represents $p \leq 0.05$, (**) represents $p \leq 0.01$. A) Average traces of evoked excitatory junction potentials (EJPs). B) Mean amplitude of EJPs (mV) $\pm$ SEM. EJPs showed that neuronal function of *Df(3R)pak3*/$pak3^{d02472}$ and *Df(3R)pak3*/$pak3^{d02472*}$ larvae were equivalent, and both were unchanged from w^{1118} controls. Both combinations were able to suppress the *spastin* null defects. Neither mini EJP (mEJP) amplitude (C), nor quantal content (D) was affected by genetic background. E) While mEJP frequency (Hz) was significantly reduced in both genetic combinations of *pak3* mutants alone, the double mutants differed

slightly in their effects. *Df(3R)pak3 spas*/*pak3*^{d02472} *spas* were no different from wild-type, but *Df(3R)pak3 spas*/*pak3*^{d02472*} *spas* were elevated and statistically significant from wild-type. Neither double mutant was distinguishable from *spastin* null larvae. Therefore, while the effects of removing both *pak3* and *spastin* are clearly distinct from the *pak3* mutant alone, it is possible that they resemble *spastin* mutants more closely than controls.